Int. J. Electrochem. Sci., 16 **(2021)** Article ID: 210632, doi: 10.20964/2021.06.32

International Journal of ELECTROCHEMICAL SCIENCE
www.electrochemsci.org

Short Communication

Optical and Electrochemical Properties of Silver-doped Yttrium Barium Copper Oxide as High-Temperature Superconducting Materials

Ping Gao

Department of Physics, Lvliang University, Lvliang, Shanxi, 033000, China
E-mail: pinggao@protonmail.com

Received: 22 March 2021 / *Accepted:* 6 April 2021 / *Published:* 30 April 2021

This work focused on electrochemical and optical properties of yttrium barium copper oxide (YBCO) and Ag-doped YBCO (Ag-YBCO) as superconducting films. The films were synthesized through conventional solid state reactions. Morphology, crystal and chemical structure, optical and electrochemical properties of synthesized films were studied at room temperature. Morphological results using FESEM analysis showed that YBCO and Ag-YBCO films surface were covered with rectangular crystal grains which grew parallel and perpendicular to the basal plane. Studying the crystal structure using XRD analysis showed that there was the orthogonal superconducting phase of Y123 before sintering processing. XRD results also showed elimination of $BaCO_3$ phase and formation of crystalline phase of Ba-Cu-O_3in sintered YBCO film and incorporation of fcc phase of Ag into the doped film. Raman analysis demonstrated the formation of oxide phases in YBCO and Ag-YBCO films. Optical analysis illustrated the formation of AgO in doped film could provide reactive atomic oxygen to the growth YBCO thin film. Study of electrochemical properties indicated that area specific resistance of Ag-YBCO was lower than YBCO electrode and electrochemical response of Ag-YBCO was more stable than YBCO response because of more electrochemical activity of silver particles of doped film in aqueous solution. Furthermore, Ag addition in YBCO film can change in the charge carrier and electronic structure in the compound due to the formation of oxygen vacancies in the CuO chains or CuO_2 planes. Therefore, the synergetic effect of high electrical conductivity and higher concentration of oxygen vacancy in YBCO and higher stability of silver particles improves the charge transfer and surface oxygen exchange in the electrode, and as a result, it can promote the electrochemical performance of doped film.

Keywords: Electrochemical properties; Silver-doped Yttrium Barium Copper Oxide; Raman spectroscopy; Electrochemical impedance spectroscopy; Cyclic voltammetry

1. INTRODUCTION

YBCO compounds as crystalline oxygen superstructure are high temperature superconductor that their family are contained compounds such as Y123 ($YBa_2Cu_3O_{7-x}$), Y124 ($YBa_2Cu_4O_y$), Y145

($YBa_4Cu_5O_{11-x}$), Y156 (YBa5Cu6O13-x), Y247 ($Y_2Ba_4Cu_7O_y$), Y257 (Y2Ba5Cu7Ox) and Y358 ($Y_3Ba_5Cu_8O_{18-\delta}$), Y3–8–11, Y5–8–13, Y7–11–18, Y13–20–23 and etc. There are many application for these compounds such as magnetic resonance imaging machines in hospitals, magnetic levitation, HTS cables, AC loss reduction in transformer and Josephson junctions [1, 2]. Moreover, studies showed the surface modification of materials lead to improve device efficiency such as corrosion inhibition, development the sensitivity of sensor, polymer adhesion and nucleation [3, 4]. Modification and preparation of metal/insulator/superconductor tunnel junctions also shows the potential as excellent model circuits for future electronic devices and perovskites. Nevertheless, YBCO compounds have yet to be used in many applications due to brittle, impurity and low mechanical and chemical stabilities [5]. Therefore, doping and modification of YBCO compounds can help to remove the problems and limitations. For example, Dadras et al. [6]reported the preparation of graphene oxide doped YBCO by sol-gel method. They showed that the graphene oxide doping led to a positive effect on superconducting properties. Zhang et al. [7] synthesized crack-free Fe-doped YBCO films using fluorine-free polymer-assisted metal organic deposition method. They also exhibited that the current carrying capability of YBCO film can improve by Fe doping.

For several decays, many techniques were found to synthesis of YBCO compounds which contained metal organic deposition, chemical solution deposition, chemical vapor deposition, thermal evaporation deposition, pulsed laser deposition, metal organic chemical vapor deposition, sol-gel processing, spray pyrolysis, wet precipitation, aerosol, freeze-drying processing and solid state reaction methods [8]. Among these methods, solid state reaction methods can provide the required condition such as oxygen flow during sintering and annealing processes for mixture the elements, diffusion and creation the oxide phases in stoichiometric and high quality crystalline compounds of YBCO [9]. Therefore, this study conducted on investigation the electrochemical and optical properties of YBCO and Ag doped YBCO as superconducting films which synthesized through conventional solid state reactions.

2. EXPERIMENTAL

2.1. Synthesis of YBCO and Ag-YBCO films

Single crystalline superconducting YBCO film was synthesized through conventional solid state reaction on Si substrate. The Y_2O_3 (99.99 %, Sigma–Aldrich), $BaCO_3$(99 %, Sigma–Aldrich) and CuO (98 %, Inner Mongolia Pulisi Chemical Co., Ltd., China) powders as precursor were homogeneously mixed in weight ratio of 1:2:3. The weights of the precursor were stoichiometrically adjusted to make YBCO compounds in accordance with the propellant chemistry principles. For Ag doping, Ag was added in 3% of the nominal composition of Cu in the resulting superconductor. Then, the mixture was transferred to the furnace and heated at a heating rate of 20°C/minutes to reach temperature of 800°C and was calculated in this temperature for 5 hours to vanish green color of mixture and accelerate the precursors decomposition. Moreover, the calcinations process in high temperature helps to oxidation, diffusion and balance of substances in prepared superconductors at stoichiometric phase. Then, the specimen was quickly cooled down to room temperature and again

calculated in flowing O_2 in at 900 °Cat heating rate of 100°C/minutes for 24 hours to totally move CO_2 in reaction. The calcined mixture was sintered in flowing O_2 in the furnace at 900 °C for 24 hours. After that, the specimen was quickly cooled down to 450°C and annealed in O_2 at 450°C for 6 hours to complete the oxidation process. Finally, the specimen was slowly cooled down to room temperature and stored in a desiccator with silica gel to avoid being exposed to atmospheric moisture.

2.2. Measurements techniques

Morphology and structure of prepared films were studied using the field emission scanning electron microscope (FESEM; JEOL Model: JSM-7001F). The crystal structures of films were characterized using X-ray diffraction technique (XRD; Rigaku Miniflex 600, Tokyo, Japan with Cu-Kα radiation, λ= 0.154 nm). Raman spectra were taken in the range of 100–800 cm^{-1} with a Raman spectroscope (Kaiser Optical Systems, Inc. RamanRxn1TMspectrom-eter) using 785nm near-infrared GaAlAs diode laser as an excitation source. The optical emission spectra of samples were recorded using spectrometers (Triax 550, JobinYvon) equipped with a 450 W xenon source.

Electrochemical impedance spectroscopy (EIS) and cyclic voltammetry (CV) measurements were performed in electrochemical cell which contained the working electrode (YBCO and Ag-YBCO), counter electrode (platinum wire) and reference electrode (Ag/AgCl) using potentiostat/galvanostat Methrom Autolab (PGSTAT 30, Eco-Chimie, Utrecht, The Netherlands). EIS analyses were carried out under open- circuit AC amplitude of 5 mV at frequency range of 10^{-1} to 10^5 Hz in 1M KOH (95%, Guangzhou Zhonglian Building Material Co., Ltd., China) as electrolyte. Cyclic voltammetry analyses in potential range from -0.9 V to 0.5 V at scan rate 50 mVs^{-1} in 0.1 M NH_4Cl (99.5%, Tianjin Bohai Chemical Industry Group Supply and Sales Co., Ltd., China) pH 5.8.

3. RESULT AND DISCUSSION

3.1 Structure and morphology characterizations of YBCO and Ag-YBCO films

Figure 1 shows the FESEM images of YBCO and Ag-YBCO films. As seen in Figure 1a, the YBCO film surface was covered with rectangular grains with an average diameter of 3.5 μm. There are the micro-cracks extending in average length of 20 μm. The grain boundaries are separated with variously-oriented crystal regions which show the grown crystals parallel and perpendicular to the basal plane.

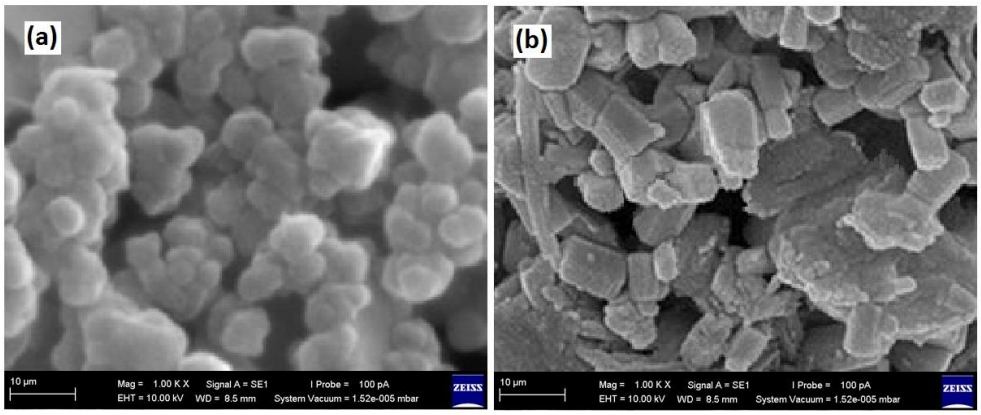

Figure 1. FESEM images of (a) YBCO and (b) Ag-YBCO films.

Figure 2 displays the XRD patterns of YBCO samples before sintering processing, sintered YBCO and Ag-YBCO films. For sample before sintering processing, XRD pattern shows the orthogonal superconducting phase of Y123 according to JCPDS card No. 01–079–0318 which revealed crystallite growth in the c-direction. This phase is unsteady at temperatures higher than 650°C [9]. Incorporation of oxygen during conventional solid state reactions is an important factor for the growth of YBCO films [10]. Studies showed that deposited YBCO films in temperature range between 650 and 750 °C in a partial pressure of oxygen displayed orthorhombic crystal structure as oxygen-deficient phase of YBCO [9, 10]. As shown in XRD pattern of sintered YBCO, thermal treatment in flowing O_2 at 900°C lead to deletion of $BaCO_3$ phase and formation of crystalline phase of Ba-Cu-O_3. XRD pattern of Ag-added YBCO film exhibits two diffraction peaks in (111) and (200) planes for fcc phase of Ag according to JCPDS card No. 00–04–0783 which indicated incorporation of Ag particles into the YBCO film.

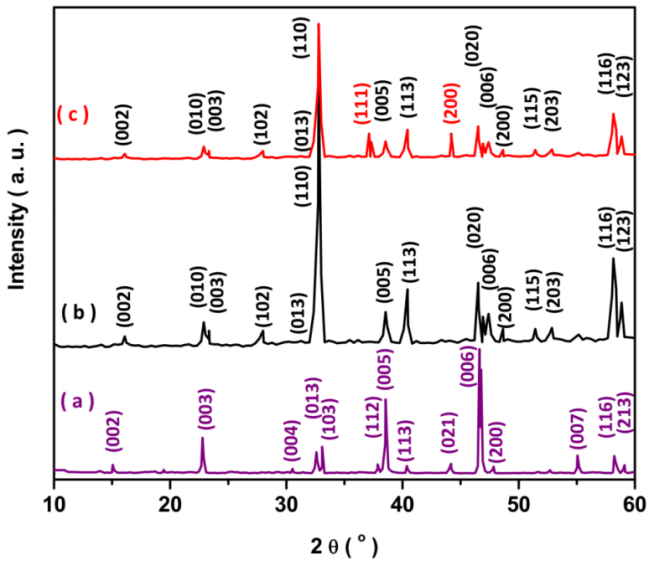

Figure 2. XRD patterns of (a) YBCO samples before sintering processing, (b) sintered YBCO and (c) Ag-YBCO films.

3.2 Raman and optical characterizations of YBCO and Ag-YBCO films

Figure 3 shows the Raman spectroscopy of prepared YBCO films in this study. As seen for YBCO film, there is a peak at 114 cm^{-1} which revealed the oscillation of Ba atoms around the c-axis [11]. The peak at 149 cm^{-1} is associated with axial stretching of the Cu(2) atoms [12]. The peak at 224 cm^{-1} attributed to the cation-oxygen network that these were broken in grain boundaries of YBCO surface. The peak at 299 cm^{-1} is related to the present of CuO compounds in the film structure. the peaks at 334 cm^{-1}, 444 cm^{-1} and 499 cm^{-1} are correlated to O(2+/3–), O(2+/3+) and O(4) modes of YBCO [13]. The low instance peak at 579 cm^{-1} is referred to the existence of cation disorder in the YBCO structure [13]. Raman spectra of Ag-YBCO film shows deactivation of O (4) peak (498 cm^{-1}) that this peak is related to oxygen stoichiometry of the YBCO films [14]. Moreover, the apical oxygen lines shifted to lower frequency.

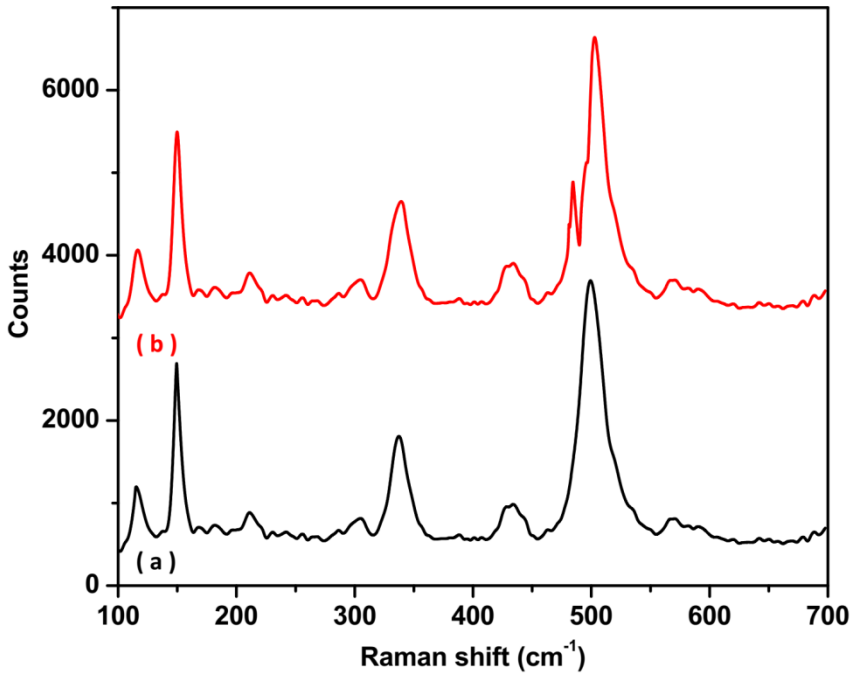

Figure 3. Raman spectroscopy of (a) YBCO and (b) Ag-YBCO films.

Figure 4 shows the recorded optical emission spectra of YBCO and Ag-YBCO films in the wavelength region from 400 to 650 nm. There are the most prominent emission lines of the various ablation products of YBCO and Ag-YBCO films such as Y (546.67 nm), Y^+ (437.58, 485.59, 488.49, 508.90 and 566.43 nm), YO (597.01, 599.02 and 601.04 nm), Ba (490.11, 553.69 and 577.91 nm), Ba^+ (413.20, 416.70, 452.59, 455.55, 490.09, 493.53, 585.55 and 614.35nm) and Cu (465.25, 510.69, 515.50 and 522.01 nm) that this observation is in agreement with the results from other optical emission spectra of YBCO [15, 16]. As seen for recorded optical emission spectra of Ag-YBCO film in the blue region, two strong emission lines of AgO at 422.0 and 429.9 nm which were attributed to

formation of AgO [17, 18]. The formation of AgO could provide reactive atomic oxygen to the growth YBCO thin film [19]. In addition, Ag addition in oxide film could enhance the oxygen content in oxide film [19, 20].

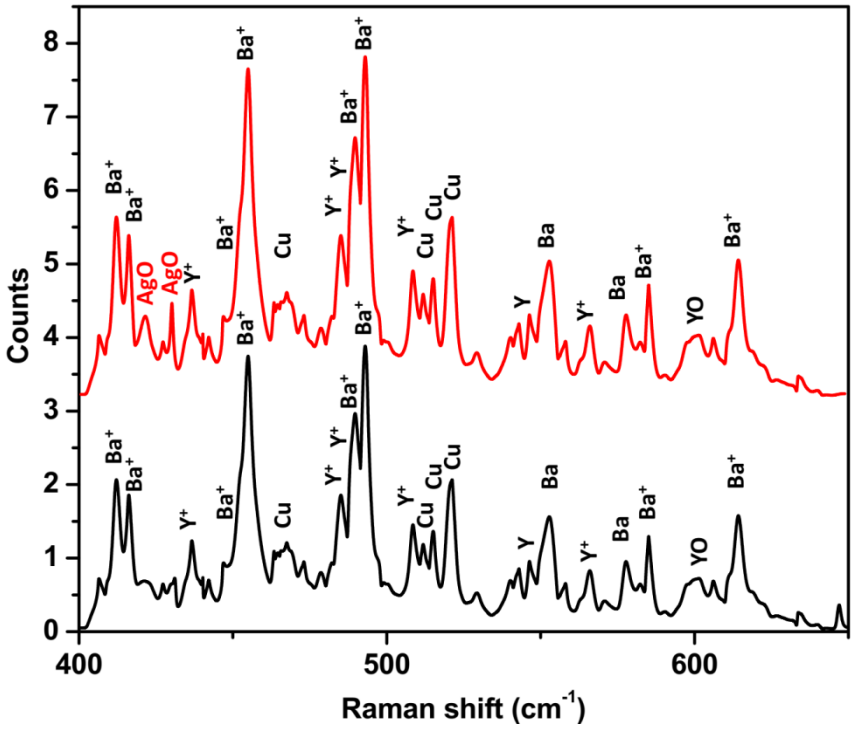

Figure 4. Recorded optical emission spectra of (a) YBCO and (b) Ag-YBCO films.

3.3 Electrochemical characterization of YBCO and Ag-YBCO films

In order to study the electrochemical properties of the YBCO and Ag-YBCO electrodes, the EIS analyses are carried out in electrochemical cells under open- circuit AC amplitude of 5 mV in frequency range of 10^{-1} to 10^{5} Hz. Figure 5a and 5b show the recorded EIS spectra of YBCO and Ag-YBCO electrodes, respectively which displaying two overlapped depressed semicircles corresponds to finite mass transfer process in oxide films/electrolyte interface at low frequency without any Warburg impedance [21, 22]. At high frequency (R_{sf}, C_{sf}), semicircle is consistent with a charge transfer process on the electrode/electrolyte interface [21, 22]. At low frequency (R_{ct}, C_{dl}), semicircle arises from oxygen reduction reaction which is dominated by oxygen adsorption-dissociation and diffusion processes. Equivalent circuit of recorded EIS spectra is shown in Figure 5c which contained R_{sf} and R_{ct} related to surface film impedance at high and low frequency, respectively and C_{sf} and C_{dl} related to capacitances at high and low frequency, respectively. In addition, ohmic resistance (R_O)in equivalent circuit is the left intercept to the real axis and total resistance (R_t) is obtained from the right intercept of the semicircle with the real axis in the EIS spectra [23]. The area specific resistance (R_S) is

obtained from the difference between R_t and R_O values [24]. The obtained R_{sf}, R_{ct} and R_S for Ag-YBCO are 0.29 kΩ, 0.58 kΩ and 66 Ω, respectively, and 0.81 kΩ, 1.24 kΩ and 98 Ω are calculated for YBCO. The results indicate R_S value of Ag-YBCO is lower than YBCO electrode which can be ascribed to the more electrochemical activity of silver particles in Ag-YBCO in aqueous solution [25]. Therefore, the synergetic effect of high electrical conductivity and higher concentration of oxygen vacancy in YBCO and higher stability of silver particles improves the charge transfer and surface oxygen exchange in the electrode, and as a result enhances the electrochemical activity [26, 27].

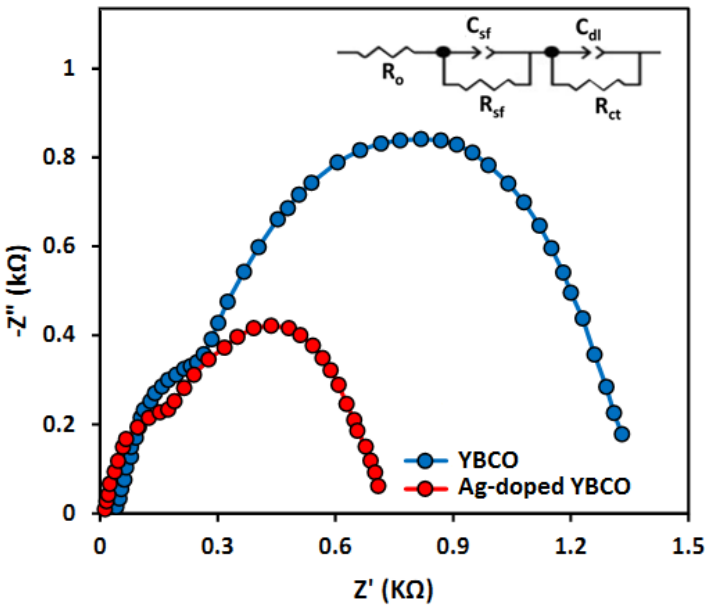

Figure 5. EIS spectra of YBCO and Ag-YBCO electrodes under open- circuit AC amplitude of 5 mV in frequency range of 10^{-1} to 10^5 Hz in 1M KOH as electrolyte. Inside figure shows an equivalent circuit of recorded EIS spectra.

Figure 6a shows the first recorded CVs of YBCO and Ag-YBCO electrodes in potential range from -0.9 V to 0.5 V at scan rate of 50mVs^{-1} in 0.1 M NH_4Cl pH 5.8. As observed, there are two symmetrical redox processes which contained well defined two cathodic peaks and two anodic peaks due to electrochemical reactions of copper species in YBCO and Ag-YBCO electrodes that it is in agreement with the results from other electrochemical reports of YBCO based electrodes [28, 29]. The first redox reaction at 0.17 V ($E(pc)_I$) and 0.24 V ($E(pa)_I$) are presented as following mechanism [28-30]:

Reaction in $E(pc)_I$: $Cu^{2+} + e^- \rightarrow Cu^+$ (1)
Reaction in $E(pa)_I$: $Cu^+ \rightarrow Cu^{2+} + e^-$ (2)

The second redox reaction at -0.21 V ($E(pc)_{II}$) and 0.01 V ($E(pa)_{II}$) are also assigned as following mechanism [28-30]:

Reaction in $E(pc)_{II}$: $Cu^{+} + e^{-} \rightarrow Cu^{0}$ (3)
Reaction in $E(pa)_{II}$: $Cu^{0} \rightarrow Cu^{+} + e^{-}$ (4)

Comparison between the recorded CVs of YBCO and Ag-YBCO electrodes in Figure 6a reveals the current of redox peaks in Ag-YBCO electrode is more than YBCO electrode. Moreover, the couple peak separation value for the first and second redox reactions of Ag-YBCO electrodes are lower than those in YBCO electrodes. It is suggested that these changes can be related to change in the charge carrier and electronic structure in the compound because of the formation of oxygen vacancies in the CuO chains or CuO_2 planes and electrostatic doping [31, 32]. It indicates that the doping of Ag into YBCO can be situated on planes of Cu_2O or chains of CuO [33]. Accordingly, the oxygen vacancies may change the valence of the Cu in YBCO film [33].

Stability of electrochemical response of both electrodes were studied through the record of continuous CVs in potential range from -0.9 V to 0.5 V at scan rate 50 mVs^{-1} in 0.1 M NH_4Cl pH 5.8. Figure 6b shows the second, 5th and 70th recorded CVs of YBCO and Ag-YBCO electrodes. As observed, the current of peaks are slightly decreased from second to 5th recorded CVs (8% and 3% for YBCO and Ag-YBCO, respectively which implied the steady and equilibrium condition in redox reaction and electrochemical response of both electrodes [30]. Furthermore, the current response of Ag-YBCO (7.4 µA after 70th recorded CVs) is higher and more stable than YBCO electrode (6.4 µA after 70th recorded CVs).

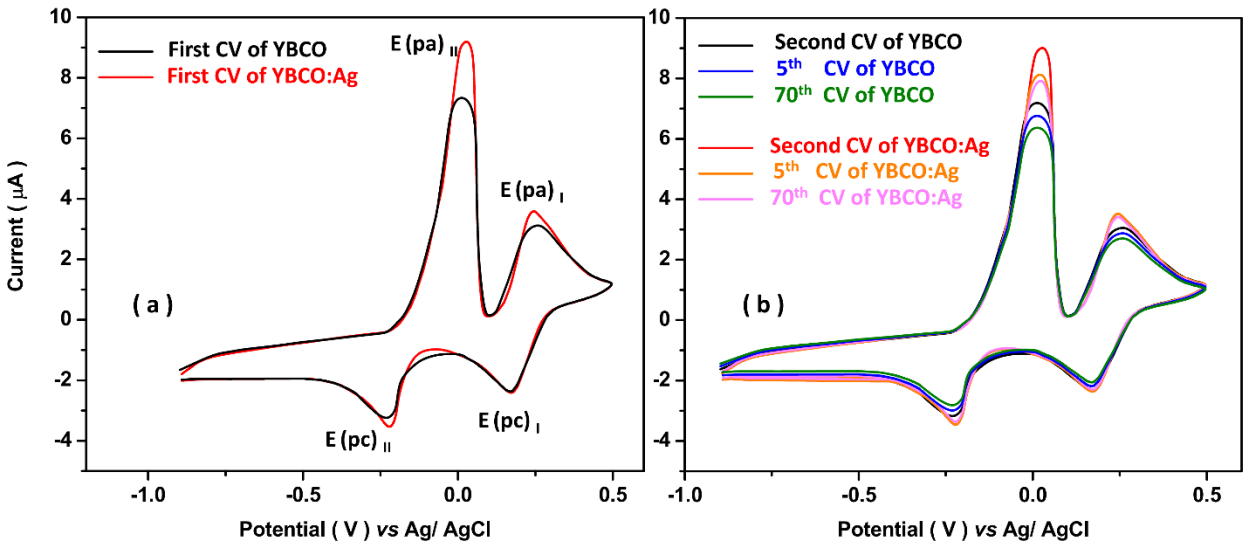

Figure 6. (a) First and (b) second, 5thand 70th recorded CVs of YBCO and Ag-YBCO electrodes in potential range from -0.9 V to 0.5 V at scan rate of 50 mVs^{-1} in 0.1 M NH_4Cl pH 5.8

4. CONCLUSION

This research revealed electrochemical and optical study on YBCO and Ag-YBCO films as superconducting materials. These films were synthesized through conventional solid state reactions on

Si substrate. The morphology and crystal structure of films were analyzed using FESEM and XRD, respectively. Chemical structure and optical studies were performed using Raman spectroscopy and optical emission spectrometry techniques, respectively. Electrochemical properties were studied via EIS and CV techniques. FESEM results showed YBCO and Ag-YBCO films were covered of rectangular crystal grains which grew parallel and perpendicular to the basal plane. XRD results presented that the YBCO sample before sintering processing had the orthogonal superconducting phase of Y123 which revealed crystallite growth in the c-direction. Structural analysis of sintered YBCO showed thermal treatment in flowing O_2 at 900°C led to elimination of $BaCO_3$ phase and formation of crystalline phase of Ba-Cu-O_3. Moreover, the XRD pattern of Ag-added YBCO film exhibited the incorporation of the fcc phase of Ag particles into the YBCO film. Raman analysis displayed the formation of oxide phase of YBCO and incorporation of Ag doped film. Optical analysis showed the formation of AgO in doped film could provide reactive atomic oxygen to the growth YBCO thin film. Results of electrochemical study indicated that area specific resistance of Ag-YBCO was lower than YBCO electrode and electrochemical response of Ag-YBCO was more stable than YBCO response which can be ascribed to the more electrochemical activity of silver particle in Ag-YBCO in aqueous solution. Furthermore, Ag addition in YBCO film led to change in the charge carrier and electronic structure in the compound because of the formation of oxygen vacancies in the CuO chains or CuO_2 planes and electrostatic doping. Therefore, the synergetic effect of high electrical conductivity and higher concentration of oxygen vacancy in YBCO and higher stability of silver particles improves the charge transfer and surface oxygen exchange in the electrode, and as a result enhances the electrochemical activity.

References

1. L. Pathak and S.K. Mishra, *Superconductor Science and Technology*, 18 (2005) R67.
2. H. Karimi-Maleh, M.L. Yola, N. Atar, Y. Orooji, F. Karimi, P.S. Kumar, J. Rouhi and M. Baghayeri, *Journal of colloid and interface science*, 592 (2021) 174.
3. Z. Savari, S. Soltanian, A. Noorbakhsh, A. Salimi, M. Najafi and P. Servati, *Sensors and Actuators B: Chemical*, 176 (2013) 335.
4. R. Savari, H. Savaloni, S. Abbasi and F. Placido, *Sensors and Actuators B: Chemical*, 266 (2018) 620.
5. R. Chaim and H. Marom, *Journal of materials science letters*, 12 (1993) 1563.
6. S. Dadras, S. Dehghani, M. Davoudiniya and S. Falahati, *Materials Chemistry and Physics*, 193 (2017) 496.
7. H. Zhang, Y. Zhao, W. Wang, M. Pan and M. Lei, *Journal of Modern Transportation*, 22 (2014) 45.
8. H. Karimi-Maleh, S. Ranjbari, B. Tanhaei, A. Ayati, Y. Orooji, M. Alizadeh, F. Karimi, S. Salmanpour, J. Rouhi and M. Sillanpää, *Environmental Research*, 195 (2021) 110809.
9. A. Harabor, P. Rotaru, N.A. Harabor, P. Nozar and A. Rotaru, *Ceramics International*, 45 (2019) 2899.
10. P. Benzi, E. Bottizzo and N. Rizzi, *Journal of Crystal Growth*, 269 (2004) 625.
11. Z. An-Min and Z. Qing-Ming, *Chinese Physics B*, 22 (2013) 087103.
12. J. Rodriguez and A. Lazo. *Synthesis of YBCO superconductor by the method of combustion reaction in solution*. in *Journal of Physics: Conference Series*. 2018: IOP Publishing.

13. H.-J. Jin, H.-K. Moon, S. Yoon, W. Jo, K. Kim, M. Kim, R.-K. Ko, Y.-S. Jo and D.-W. Ha, *Superconductor Science and Technology*, 29 (2016) 035016.
14. A. Kujur, K. Asokan and D. Behera, *Thin solid films*, 536 (2013) 256.
15. J. Göres, P.-J. Kung, D. Fenner and J. Budnick, *Review of Scientific Instruments*, 68 (1997) 170.
16. V. Tsaneva, T. Donchev, R. Tomov, D. Ouzounov, A. Veneva and T. Nurgaliev, *Vacuum*, 48 (1997) 803.
17. A.M. Auti, N.P. Narwade, N.M. Deshpande and D.P. Dhotre, *Journal of Biosciences*, 44 (2019) 114.
18. A. Nwanya, P. Ugwuoke, B. Ezekoye, R. Osuji and F. Ezema, *Advances in Materials Science and Engineering*, 2013 (2013) 1.
19. R. Pinto, P. Apte, K. Adhi, S. Ogale, D. Kumar and M. Hegde, *Journal of applied physics*, 78 (1995) 5204.
20. D. Kumar, S. Oktyabrsky, R. Kalyanaraman, J. Narayan, P. Apte, R. Pinto, S. Manoharan, M. Hegde, S. Ogale and K. Adhi, *Materials Science and Engineering: B*, 45 (1997) 55.
21. M. Ebrahimzadeh, M. Gholami, M. Momeni, A. Kosari, M. Moayed and A. Davoodi, *Applied surface science*, 332 (2015) 384.
22. R. Tatara, P. Karayaylali, Y. Yu, Y. Zhang, L. Giordano, F. Maglia, R. Jung, J.P. Schmidt, I. Lund and Y. Shao-Horn, *Journal of The Electrochemical Society*, 166 (2018) A5090.
23. L. Wang, J. Zhao, X. He, J. Gao, J. Li, C. Wan and C. Jiang, *International Journal of Electrochemical Science*, 7 (2012) 345.
24. J. Shi and X. Xue, *Journal of Applied Electrochemistry*, 44 (2014) 683.
25. B.J. Plowman, B. Sidhureddy, S. Sokolov, N.P. Young, A. Chen and R. Compton, *ChemElectroChem*, 3 (2016) 1039.
26. G. Kim, S. Wang, A. Jacobson, L. Reimus, P. Brodersen and C. Mims, *Journal of Materials Chemistry*, 17 (2007) 2500.
27. D.O. Perevezentseva, E.A. Vaitulevich and V.I. Bimatov, *Oriental Journal of Chemistry*, 34 (2018) 1130.
28. C. ShanáLim and C. KiangáChua, *Journal of Materials Chemistry A*, 3 (2015) 8346.
29. E.N. Izakovich, V.M. Geskin and S.V. Stepanov, *Synthetic Metals*, 46 (1992) 71.
30. M. Nazarudin, Z. Zainal, W. Tan, I. Hamadneh and E. Kadri, *International Journal of Electrochemical Science*, 7 (2012) 2965.
31. E.S. Alaghbari, Z. Zainal, M. Zidan and T.W. Tee, *International Journal of Electrochemical Science*, 8 (2013) 2034.
32. R. Poloni, A.L. Mariano, D. Prendergast and J. Garcia-Barriocanal, *The Journal of Chemical Physics*, 149 (2018) 234706.
33. P.d. Azambuja, P. Rodrigues Júnior, A.R. Jurelo, F.C. Serbena, C.E. Foerster, R.M. Costa, G.B.d. Souza, C.M. Lepienski and A.L. Chinelatto, *Brazilian Journal of Physics*, 39 (2009) 638.